

# Near-Field Optical Microscopy of Surface Plasmon Polaritons Nano-Optics

**Víctor Coello**

*Centro de Investigación Científica y de Estudios Superiores de Ensenada BC, Unidad Monterrey, Ángel Martínez Villarreal 425, Col. Chepevera, Monterrey Nuevo León. C.P. 64030*

Near field optical microscopy techniques can be employed to characterize surface plasmon polaritons phenomena. These studies have set the stage for the current surge in the nano-optics field. In this chapter experiments and numerical developments conducted to the understanding of this area are outlined. Furthermore a scanning near-field microwave microscope is presented as an alternative technique that is reliable enough to be used as a check of potential (two-dimensional) micro-components and eventually for micro and nano-circuits.

**Keywords** Near field optical microscopy, surface plasmon polaritons, evanescent waves.

## 1. Introduction

Current progress in optics of surface plasmon polaritons (SPPs) [1] offers new and broad ranges of scientific and technological perspectives. For instance, SPP are applied to efficiently channel light using scatterers in subwavelength structures [2]. This could lead, in principle, to a novel generation of nano-optics circuits. This attractive idea is based on the similitude between SPPs and waves propagating in planar waveguides since both are two dimensional waves propagating in the surface. However, one has to born in mind that this similitude stops here. SPP field have its maximum intensity at the surface plane, in contrast with the (two dimensional) guided waves in integrated optics. Moreover, it is easier to scatter SPP out of the plane than along to it. Actually, as a SPP field is strongly confined in the direction perpendicular to the surface, a direct observation of SPP localization is only possible by means of scanning near-field optical microscopy (SNOM) techniques [3]. Near-field optical microscopy of SPPs has corroborated the existence of both weak and strong SPP localization [4]. However a local control (at a desirable surface place) of such SPP optical enhancement started to take form only with the birth of the two-dimensional optics of SPPs [5]. The idea is to manipulate and direct SPP beams along the surface plane by using *artificially* created nano-components. Thus artificially fabricated SPP nano-optical *structures* such as nano-bumps acting as a nanolens (focusing the SPP field) have been investigated for different films and wavelengths [5]. In general, working in optics in the sub wavelength regime is not trivial. Structures smaller than the wavelength, may not lead to the expected results and the investigations revealed several features such as wavelength dispersion and stability (with respect to geometric parameters) of the components that still have to be elucidated. The studies are well complemented by using numerical simulations. For example, a scalar multiple-scattering approach was used for simulations of SPP optical nano-components [5] and photonic band gap structures formed by sets of individual scatterers [6]. Later, the approach has been extended into a vector dipolar multiple-scattering theory [7] and used to calculate SPP scattering produced by band-gap structures and for modelling the operation of a SPP interferometer formed by equivalent scatterers lined up and equally spaced [8]. Another interesting approach, for the sub-wavelength studies, is the use of the microwave radiation. The first proposal for a scanning near field microwave microscope (SNMM) came from Ash and Nichols in 1972 [9]. Since then, the technique has demonstrated its potential in areas such as magneto-resistivity characterization, superconductivity, and dielectric constant of individual samples [10]. Recently, it was proposed a simple SNMM designed to adopt dissimilar illumination operations modes and with capabilities for studies of potential two-dimensional optical devices [11]. In this work, I

present an overview of some of the problems, developments and current progress related with our research in the surface polariton nano-optics. I begin with an introduction to SPPs in section 2 followed by a brief discussion of SNOM concepts in section 3. Experimental results on weak and strong SPP localization exhibited in relative smooth and rough metallic surfaces will be presented in section 4. Section 5 describes a multiple scattering model that was used for simulation of SPP optical nano-components. The effects of SPPs in artificially nanostructured surfaces will be discussed in section 6. A near-field microwave technique used as an experimental approach for checking potential two-dimensional nano-SPP components will be analysed in section 7. Finally, in section 8, applications and further investigations of the surface plasmon nano-optics are outlined.

## 2. Surface plasmon polaritons

SPPs are collective excitations of the electrons at the interface between a conductor and an insulator. This leads to oscillatory longitudinal motion of the electrons along the surface-plane that has associated an electromagnetic field with a wave vector  $\beta$  and that decays exponentially in the perpendicular direction of such an interface (Fig. 1). For this reason, SPPs exhibit a high sensitivity to surface properties such as roughness and surface adsorbates [1]. SPPs are responsible for exciting phenomena such as surface enhanced Raman scattering [1], SPP weak and strong (Anderson) localization [4] and the extraordinary transmission of light through nanoholes [12]. As it is characteristic for evanescent fields, for the SPP to exist, the wavenumber associated with it must be larger (in absolute value) than the light wavenumber in the neighbour media [1]. The electromagnetic derivation of the SPP modes results in the fact, that such modes are possible only for *p*-polarization of light (TM-waves), since *s*-polarized waves (TE-waves) do not satisfy the boundary conditions. Due to their electromagnetic nature, SPPs can diffract, reflect, and interfere. Those properties are clearly exhibited in the course of SPP scattering. Scattering of SPPs is usually caused by randomly placed surface imperfections (as even the most carefully prepared surfaces are not completely flat). Hereafter, we should distinguish between two kinds of SPP scattering: *inelastic and elastic SPP scattering*. For *inelastic scattering*, we will consider, propagating field components scattered away from the surface decreasing the total energy stored in SPPs. *Elastic scattering* occurs when SPPs are scattered by surface imperfections *along the surface plane*, i.e. into other SPPs preserving the total SPP energy.

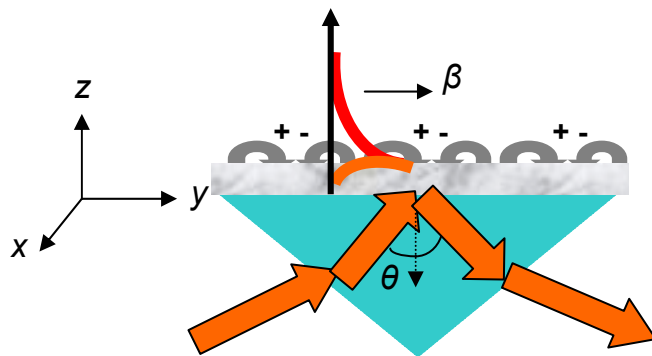


**Fig. 1** Schematic representation of SPPs excitation.

### 2.1. Surface polaritons properties.

In order to show some of the SPP characteristics, let us consider the interface between two semi-infinite media as air-metal. The SPP electric field existing in such a system (Fig. 1) can be represented as:

$$E(x, y) = E_0 e^{i\beta \cdot \hat{x}} \cdot e^{-\gamma \cdot \hat{z}}, \quad (1)$$

which is an electromagnetic mode propagating in the  $x$ -direction along the surface and with an exponential decay perpendicular ( $z$ -direction) to it (Fig. 1). The SPP wave vector,  $\beta$ , and the air decay constant,  $\gamma$ , are derived through the use of Maxwell's equations and the boundary conditions, yielding the expressions:

$$\beta = \frac{2\pi}{\lambda_0} \sqrt{\frac{\epsilon_m}{1 + \epsilon_m}}, \quad \gamma = \sqrt{\beta^2 - k_0^2}, \quad (2)$$

being  $\lambda_0$  the incident wavelength,  $\epsilon_m$  the dielectric constant of metal, and  $k_0$  the incident wave number. The SPPs modes have an exponential decay into each of the media, being then the SPP decay constant,  $\gamma_m$ , in the metallic medium given by:

$$\gamma_m = -\sqrt{\beta^2 - \epsilon_m k_0^2}. \quad (3)$$

Other important SPP characteristics are the *SPP wavelength*,

$$\Lambda_{SPP} = \frac{2\pi}{\beta}, \quad (4)$$

the *propagation length* i.e.: the length at which the intensity decreases to  $1/e$  (along the surface),

$$L_{SPP} = \frac{1}{2\beta_{im}}, \quad (5)$$

with  $\beta_{im}$  being the imaginary part of  $\beta$ , and finally, *the penetration depth* i.e.: the length (perpendicular to the surface) at which the field amplitude decrease to  $1/e$ , and that is given by:

$$d_1 = \frac{1}{\gamma} \text{ (air)}, \quad d_2 = \frac{1}{\gamma_m} \text{ (metal)}. \quad (6)$$

## 2.2 Excitation of SPPs

Attenuated total reflection (ATR) is the most common technique for excitation of SPPs [1]. The configuration is simple, in addition to the above-mentioned air-metal interface, one should adapt, as a coupler, a dielectric medium of dielectric constant  $\epsilon_3 > 0$ . As indicated by the name, light impinging the interface is totally reflected but yet attenuated, since some of the photons are converted into SPPs. A setup for generating SPPs using ATR is the Kretschmann configuration shown in Fig 1. There the light passes through a prism, at an angle of incidence greater than the critical for the prism, which means that total reflection occurs at the prism-metal interface. At total reflection, an evanescent field is induced, which is able to penetrate the metal film and excite a surface plasmon at the metal-ambient interface. One can find the SPP resonance condition by varying the wavelength or the angle of the incident light. The most popular choice is to vary the latter parameter. In the angular case, monochromatic light is used and the intensity of reflected light is measured as a function of the incidence angle  $\theta$ . At a specific angle,  $\theta = \theta_{spp}$ , an intensity drop occurs, which indicates that the system is in resonance. The angular spectra analysis of SPP excitation allows one to deduce the SPPs characteristics parameters necessities for SPPs studies.

## 3. Scanning near field optical microscopy

The above mentioned way of indirect SPP-field measurements undergoes a drastic change, when in early 70's an idea proposed by Syngé in 1928 [13] about overcoming the diffraction limit of resolution [14] was brought into an experiment [9]: The scanning near-field optical microscopy. The operational

principle of such microscopy involves illumination of a sample through a sub-wavelength sized aperture while keeping the aperture sample distance less than half of the wavelength used. Therefore, the light does not have the opportunity to diffract before it interacts with the sample, and the resolution does not depend on the wavelength but on the aperture diameter. The image is obtained by scanning, at a nanometric distance, the aperture along the sample and simultaneously recording its optical response with the help of conventional optical detection techniques. The success of the new kind of imaging system instigated the advent of new configurations attempting to improve the technique as well as to adapt it to specific needs (a review of SNOM configurations can be found in Ref. [3]). However for all numerous SNOM versions, the fundamentals of this microscopy are found in the detection of evanescent fields [3]. The Photon Tunneling SNOM (PT-SNOM) [15], in which an uncoated fiber tip is used to probe an evanescent field of the light being totally internally reflected at the sample surface, is so far the most suitable technique for local and unobtrusive probing of the SPP field. The combination of a PT-SNOM with a shear-force feedback system [5] provides a high resolution system able to maintain tip-sample distances on the nanometer scale (~5 nm), as well as the possibility for imaging simultaneously topography and optical signal. The last feature is indispensable when studying SPP intensity distributions, since it allows us to relate surface topography and the resulting near-field SPP image.

#### **4. Near-field microscopy of surface plasmon polaritons: Localization phenomena**

SPP localization is a basis for many SPP phenomena such as: Surface enhanced Raman scattering, second harmonic generation, and nano-photonics devices. Near-field microscopy provides direct evidence of SPP localization. Localization of light is an exciting phenomenon which is entirely originated due to coherent (elastic) multiple scattering and interference in a random media. Light localization will occur if the mean free path becomes smaller or on the order of  $\lambda/2\pi$ , where  $\lambda$  represents the illumination wavelength. The effect was conceived in base of two important developments in the well known phenomenon of electron localization (Anderson localization): a) the electron localization idea was formulated as an interference effect in multiple scattering, and b) a new phenomenon called weak localization was observed. Representing two dimensional waves, SPPs may be used to study localization phenomena as a consequence of the strong scattering that a SPP undergoes in a surface with a relatively large roughness [4].

##### **4.1 Weak localization of SPPs.**

SPP weak localization (or enhanced backscattering) [18] is considered a precursor of the effect of strong SPP localization. It is also an interference effect in multiple scattering, but not as dramatic as strong SPP localization. Weak localization has been theoretically well documented since about 20 years ago [19]. The physical origin of this two-dimensional phenomenon is the same as that of the enhanced backscattering in three dimensions: the waves which travel along the same light path in opposite directions will always have the same phase and interfere constructively only in the directions of pure backscattering. In general, from a complicated SPP interference pattern, the presence of the backscattered SPP is deduced from the appearance of horizontally oriented fringes with a period equal to half the SPP wavelength in the recorded optical image. Using a PT-SNOM, in the middle of 90s, SPP optical fields were directly probed [4,5]. There, topographical images taken at a surface area of a silver film showed a relatively smooth surface. The recorded near-field optical images exhibited interference between the excited and scattered surface polaritons. Such phenomenon was related to weak localization of SPPs caused by multiple scattering in the surface plane (Fig. 2).

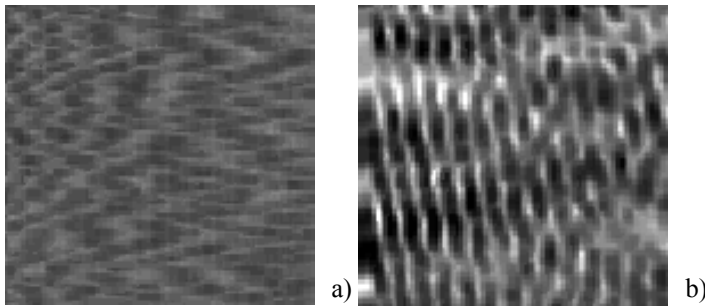


**Fig. 2** Gray-scale topographical a) and near-field optical b) images of  $2.0 \times 2.5 \mu\text{m}^2$  taken at a smooth surface silver film. The average relative roughness of the topographical image is 11 nm. The optical images is presented in a scale corresponding to  $\sim 250\text{-}550 \text{ pW}$  b) of the detected optical signal.

#### 4.2 Strong localization with rough films.

Direct observation of SPP localization was reported in the form of bright round spots with an enhancement ratio up to 5 times the background signal [4, 5, 17]. The spots positions resulted to be angle dependent and not correlated to surface topography. The observations were related to strong SPP localization in the sample surface studied. In general, those works showed a phenomenon quiet difficult to achieve since even for artificially created rough-films it is not an automatic effect. In other words, it is not simple to find media with conditions for getting short mean free paths. One cannot make the volume fraction of scatterers larger and larger, since this leads not only to elastic but also to inelastic SPP scattering. Apparently, to optimize the amount of scattering, it is necessary a large volume of scatterers whose sizes should approximately correspond to one SPP wavelength,  $\lambda_{\text{SPP}}$ . Scatterers smaller (in size) than  $\lambda_{\text{SPP}}$  are necessary for the near-field interactions responsible of the SPP confinement whereas those bigger than  $\lambda_{\text{SPP}}$  would result in strong multiple scattering indispensable for the SPP localization to occur. The surface films [4, 5, 17] were thermally deposited on the base of a glass prism which was previously covered with a sublayer of colloidal gold particles ( $\sim 40 \text{ nm}$ ) dried up in atmosphere. Therefore, the introduced surface roughness was randomly distributed along the sample surface (Fig. 3a). The elongated appearance of the particles (Fig. 3a) was probably induced by an asymmetrical shape of the fiber probe tip (taking the relatively large cone-angle into account) and/or a tilt of the fiber axis with respect to the normal direction. The near-field optical image shows the aforementioned bright spots (Fig. 3b) that were related to the phenomenon of strong SPP localization.

### 5. Theoretical Model

SPP localization may result in several advantages in nanoscience if this phenomenon could be generated in a controlled form e.g. by focusing SPP at a desirable point. A good alternative, in order to obtain the most appropriated experimental parameters, is the use of numerical simulations. Scattering of SPPs caused by surface imperfections has been considered in many theoretical papers [20 and references therein]. In general, the outcome of the investigations indicates that modelling the elastic SPP scattering is far from being trivial since even a simple case such as single scattering by an individual round homogeneous scatterer requires elaborated numerical simulations [20]. However, from the experimental work, it was observed that the elastic SPP scattering can be considered to be approximately isotropic [2,5]. Isotropic scatterers, in fact, were pointed out as a limiting case of small scatterers in a rigorous consideration of SPP scattering [20]. Taking this into account, an elastically scattered SPP can be approximated by a cylindrical SPP, which is described by the Hankel function with the lowest angular number ( $m = 0$ ) and with the wavenumber determined by the same dispersion relation as for a plane SPP [5].

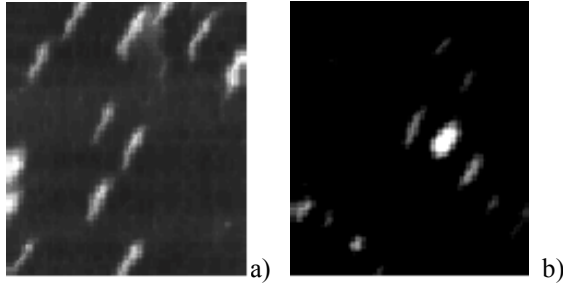


**Fig. 3** Gray-scale topographical a), and corresponding near-field optical b) images of  $4.3 \times 4.9 \mu\text{m}^2$  obtained at a relative rough gold film. The average relative roughness of the topographical image is 120nm a) nm. The optical image is presented in a scale corresponding to  $\sim 1 \cdot 10^{-1}$  nW of the detected signal.

The idea is based in two main assumptions:

1. The elastic SPP scattering is dominant with respect to the inelastic scattering.
2. The SPP scattered by each scatterer represents an isotropic cylindrical SPP.

Thus, the total SPP field at an arbitrary point  $r$ , which does not coincide with the position of any scatterer, is according to [5] given by:

$$E(r) = E_0(r) + \sum_{j=1}^N \alpha_j E(r_j) G(r, r_j), \quad (7)$$

where  $E_0(r)$  is the incident field,  $\alpha_j$  is the effective polarizability of the  $j$ th dipole,  $E(r_j)$  is the self-consistent field at the site of the  $j$ th dipole, and  $G(r, r_j)$  is the field propagator, describing the propagation of the scattered field from the  $j$ th dipole located at the source point  $r_j$  to the observation point  $r$ . The self consistent field to each dipole  $E(r_j)$  can be determined as:

$$E(r_j) = E_0(r_j) + \sum_{l=1, l \neq j}^N \alpha_l E(r_l) G(r_j, r_l). \quad (8)$$

The total field at the site of the dipole  $j$  is the incoming field at the site of the scatterer and the sum of the scattered fields from all dipoles surrounding dipole  $j$ . The field in eq. (8) then has to be inserted into eq. (7) to find the total field at a point in the plane. The field propagator is given as:

$$G(r, r_j) = \frac{i}{4} H_0^{(1)}(\beta |r - r_j|), \quad (9)$$

where  $H_0^{(1)}$  is the zero-order Hankel function of first kind and  $\beta$  is the propagation constant for the SPPs given by eq. (2).

The Hankel function first kind of order  $n$  is defined as

$$\begin{aligned} H_n^1(\beta |r - r_j|) &= J_n(\beta |r - r_j|) + iY_n(\beta |r - r_j|) \\ &= J_n(\beta |r - r_j|) + i \frac{J_n(\beta |r - r_j|) \cos(n\pi) - J_{-n}(\beta |r - r_j|)}{\sin(n\pi)}, \end{aligned} \quad (10)$$

where  $J_n(\beta |r - r_j|)$  is the Bessel function of the first kind and  $Y_n(\beta |r - r_j|)$  is the Bessel function of the second kind, and  $n$  is the order. Often it is appropriated and easier to use the farfield approximation for the Hankel function. The farfield approximation corresponds to large values of the argument [20]:

$$H_0^{(1)}(\beta|r-r_j|) \approx \sqrt{\frac{2}{\pi}} e^{-i\frac{\pi}{4}} \frac{e^{i\beta|r-r_j|}}{\sqrt{\beta|r-r_j|}}. \quad (11)$$

The calculation of eq. (8) involves a system of  $N$  homogeneous linear equations that can be solved with usual algebra methods. The estimation of the magnitude of  $\alpha$ , the effective polarizability of the individual scatterers, was done by fitting  $\alpha$  such that the calculated interference pattern generated by an individual scatterer had the same contrast of an experimental (near-field) intensity distribution generated in analogue form. It was found that a value of  $\alpha=3$  results in a good agreement between the calculated and the experimentally observed contrast (Fig. 4). Despite the apparent success, the model has some limitations, one of them being that the effective polarizability of an individual scatterer is a phenomenological quantity which is difficult to relate to scatterers parameters (e.g. size, susceptibility, etc.). Such an approach, therefore, was extended into a vector dipolar multiple scattering theory [7].

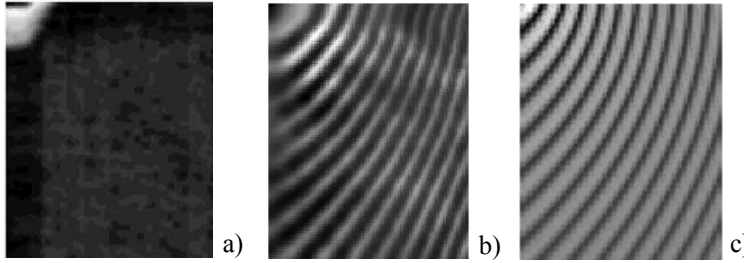


**Fig. 4.** Gray-scale topographical (a) and near-field optical (b) images of  $3 \times 4 \mu\text{m}^2$  along with the corresponding representation (c) of the calculated intensity distribution for the effective polarizability  $\alpha = 3$ . The experimental images were obtained with the polariton excited at the wavelength of 633 nm along a silver film. The average relative roughness of the topographical image is 96 nm.

### 5.1 Vectorial Model

The model is based on the following. When light is incident on a surface with scattering objects, the objects can be modelled as sphere-shaped dipoles. These dipoles scatter light as shown in Fig. 5. The Green tensor consists of a direct part, an indirect part and a part describing the SPP to SPP scattering. The direct propagation describes the scattered SPPs propagating directly from the dipole to the probe, the indirect propagator describes the scattered SPP that is reflected on the surface, and the SPP to SPP part describes the SPP to SPP scattering. The Green tensor can therefore be split into three parts:

$$G(r, r') = G_{SPP}(r, r') + G_{direct}(r, r') + G_{indirect}(r, r'). \quad (12)$$

When the distance between the scatterers is large and the radius and height of observation point is small, the incident angle on the surface for the indirect propagating part is close to  $90^\circ$ . This means that the reflected light changes phase with  $\pi$  in the reflection. Therefore, both, the direct and indirect propagating parts will be out of phase, when they meet at the other scatterer, and the overall contribution will be zero. The distances are assumed large here, so only the SPP to SPP scattering needs to be considered. As for the scalar model, the incoming plane wave is scattered into cylindrical waves at the site of the scatterers, and the field propagator is again described with the Hankel function. According to [7] the Green tensor for SPP to SPP scattering is constructed as:

$$G_{SPP}(r, r') \approx -i \frac{\beta}{2} \frac{e^{-\sqrt{\frac{\epsilon_1}{-\epsilon_2}} \beta(z+z')}}{\epsilon_1(-\epsilon_2)} \left( 1 - \frac{\epsilon_1^2}{\epsilon_2^2} \right) \frac{\epsilon_1 + \epsilon_2}{\epsilon_1 \epsilon_2}.$$

$$H_0^{(1)}(\beta_\rho) \left( \hat{z}\hat{z} - \frac{\epsilon_1}{\epsilon_2} \hat{\rho}\hat{\rho} + (\hat{z}\hat{\rho} - \hat{\rho}\hat{z})i\sqrt{\frac{\epsilon_1}{\epsilon_2}} \right), \quad (13)$$

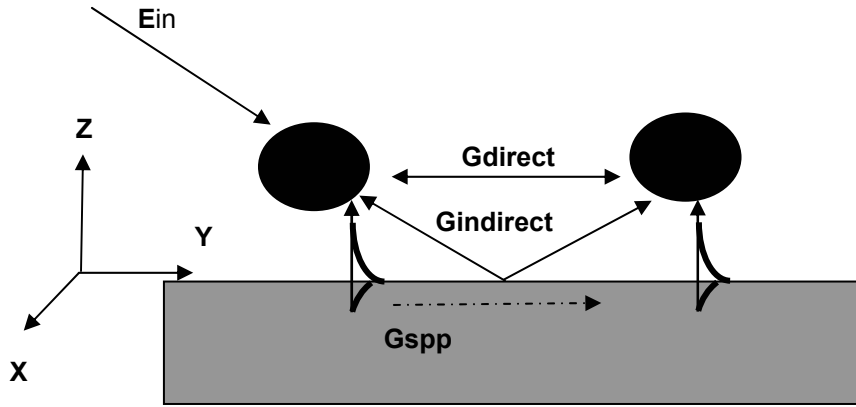


Fig. 5. Schematic representation of a dipole-dipole interaction.

where  $\epsilon_1$  and  $\epsilon_2$  are the dielectric constants for air and the metal, respectively,  $\hat{z}$  is a unit vector perpendicular to the surface,  $\hat{\rho}$  is a cylindrical in-plane unit vector,  $H_0^{(1)}$  is the zero order Hankel function of first kind, and  $\beta$  is the SPP wave vector.

With the Green's tensor determined in eq. (12) one thing is already clear. The propagation included in the Green tensor varies in different directions. This is the basic concept in the vectorial model opposed to the scalar model, in which the properties of the matter are the same in all directions. Another quantity that varies in directions in the vectorial model is the polarization. Here each nanoparticle is treated as a dipolar scatterer, and the total polarization is therefore a sum of the polarization from the scatterer itself and the surrounding scatterers. The polarization of the  $i$ 'th scatterer therefore takes the form given in ref. [7].

$$P_i = \alpha \cdot E_0(r_i) + \frac{k_0^2}{\epsilon_0} \sum \alpha \cdot G(r_i, r_n) \cdot P_n, \quad (14)$$

where  $\alpha$  is the polarizability of the scatterers. In the polarizability  $\alpha$  the surface dressing is included. This effect describes the coupling of the dipole to itself through reflection in the surface.  $E_0(r_i)$  is the incoming field at the site of scatterer  $i$ ,  $k_0$  is the wave vector of the incoming field in the space,  $G(r_i, r_n)$  is the Green tensor on the form of eq. (13). In the vectorial model the polarizability is a tensor, describing the polarizability effect in each direction [7].

$$\alpha = \left( I - k_0^2 \frac{\alpha_0}{\epsilon_0} \cdot G^S(r, r') \right)^{-1} \cdot \alpha^0. \quad (15)$$

Where  $\alpha^0$  is the free space polarizability tensor given as

$$\alpha^0 = \epsilon_0 I 4\pi a^3 \frac{\epsilon_2 - 1}{\epsilon_2 + 2}, \quad (16)$$

where  $I$  is the unit dyadic tensor. Eq (15) is valid when the long-wavelength electrostatic approximation has been used. In this approximation, it is assumed that the field is constant within the considered range that is the size of the scatterer. For this approximation to be valid the wavelength must be much bigger than the size of the scatterer. If the image dipole approximation is used on  $G^s(r, r')$  in eq. (15) the following result is obtained for the polarizability tensor of eq. (14).

$$\alpha \approx \left[ \frac{\varepsilon_2 - 1}{\varepsilon_2 + 1} \cdot \frac{\varepsilon_2 - 1}{\varepsilon_2 + 2} \left( \frac{1}{8} \hat{x}\hat{x} + \frac{1}{8} \hat{y}\hat{y} + \frac{1}{4} \hat{z}\hat{z} \right) \right]^{-1} \cdot \alpha^0. \quad (17)$$

It should be mentioned that the dipole approximation assumes that the phase delay of the field, when it moves over the scatterer, is negligible. Mathematically this means  $e^{k \cdot r} \cong 1$  for a given field. This means again that the size of the scatterer should be smaller than the wavelength, which is the main assumption in the model. When eq. (17) has been used in eq. (14) to determine the polarization, the final step is to calculate the field outside the scatterer as a selfconsistent field:

$$E(r) = E^0(r) + \frac{k_0^2}{\varepsilon_0} \sum_n G(r, r') \cdot P_n. \quad (18)$$

## 6. Nano optics of surface plasmon polaritons

Two-dimensional optics of surface plasmon polaritons is an exciting novel area. In this context, there exists a revolution in scientific and technological aspects in specific phenomena such as enhancement of an optical signal at a desirable surface place [5], waveguiding of SPP [23], and in a more general form in integrated optics. Experimental observations on nano-bumps acting as a nano-lens (focusing the SPP field) yielded conclusions about optimal parameters for a good efficiency of SPP nano components. The observations suggested that nano scatterers sufficiently large in size and with smooth borders maximize their strength and preserve an adiabatic perturbation. Thus, some of the first plane (Fig. 6) and corner square [2] nano mirrors were successfully reported.

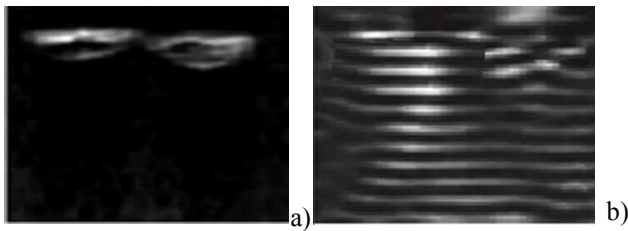


**Fig. 6.** Gray-scale topographical a) and near-field optical images b)  $4.4 \times 4.3 \mu\text{m}^2$  of a potential plane nano-mirror. In the figure, the SPP travels from bottom to top.

The advent of new investigations produced also the developments, among other devices, of SPP waveguides, beamsplitters and interferometers. In the multiple efforts of a better understanding of the SPP nano optics, a particular case of an experimentally developed SPP interferometer [24] formed by equivalent scatterers lined up was used as a check of the vectorial model aforementioned [25]. In order to numerically build step by step such an SPP interferometer first, it was investigated the in-plane scattered field created by a  $5\text{-}\mu\text{m}$ -wide Gaussian SPP beam ( $\lambda=750 \text{ nm}$ ) of a unit amplitude impinging on an equally spaced line of scatterers which acted as a beam-splitter. The SPP interferometer was completed by adding a second beam impinging at the incident angle of  $-\theta_0$  (Fig. 7a-d). The two outputs beams, which result from the interaction of the incident beams with the beam splitter, vary as a function of an

introduced phase shift,  $\varphi$ , in the incident beams (Fig. 7a-d) in a fashion that is very similar to the experimental results [24]. That it to say, switching from one side to another of the beam-splitter.

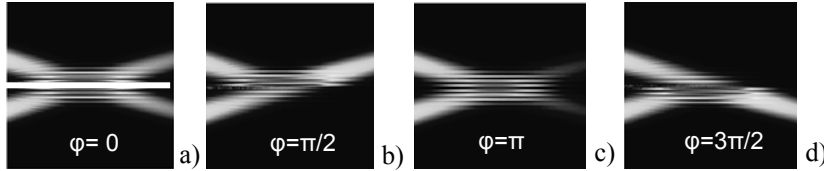


**Fig. 7.** Gray Scale representation of the total field intensity distributions in an area of  $50 \times 50 \mu\text{m}^2$  calculated for a SPP interferometer composed of 200 nanoparticles with radius of 64 nm and for the wavelength of 750nm. The angle of the incident field was set at  $\pm 16^\circ$  with regard to the normal of the line of scatterers (white line in a) ). The SPP maps have been calculated for a relative phase shifts between the incident fields of  $\varphi=0$  a),  $\varphi=\pi/2$  b),  $\varphi=\pi$  c),  $\varphi=3\pi/2$  d).

## 7. Two-dimensional optics with surface electromagnetic microwaves

In the microwave range the mechanical designs as well as the precision requirements are not as demanding as in the optical range. Taking advantage of that fact, experimental approaches for a wavelength,  $\lambda$ , of 2.85 cm. were proposed as a check of potential (two-dimensional) nano-components [11]. Several spheres were aligned keeping approximately  $\lambda/2$  distance of separation between them. Thus, distinct two-dimensional microwave components were fabricated e.g.: a 5-scatterer two-dimensional line mirror (Fig 8a,b), and a curved mirror focusing that reflected signal at 2.5 cm distance from the mirror (Fig 9a,b).

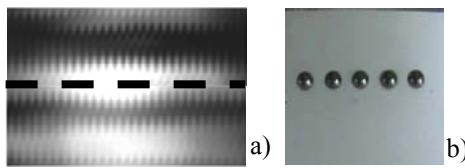


**Fig. 8.** Gray-scale near-field image of  $4.5 \times 10 \text{ cm}^2$  a) due to the elastic scattering of an evanescent microwave mode travelling from bottom to top a) on the line of scatterers placed along a wax surface prism and corresponding surface digital picture b). The dot line in a) helps to distinguish the boundary of evanescent wave and line of spheres interaction.

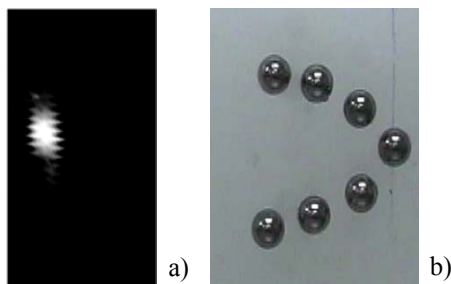


**Fig. 9.** Gray-scale near-field image of  $4 \times 6 \text{ cm}^2$  due to the elastic scattering of an evanescent microwave mode travelling from left to right on the parabolic line of scatterers placed along a wax surface prism a), and corresponding surface digital picture (not in scale) b).

The image for the line mirror showed the interference between a specular reflected evanescent microwave and the incident one. The behaviour, for the line mirrors, was not as good as it had to be. For example in Fig 8a,b) the line mirror does not completely backward reflect the incident evanescent field (travelling from bottom to top in the horizontal position) as one would expect from a normal incidence. Concerning the focusing mirror (Fig. 9a,b), ideally a focusing mirror should consist of scatterers placed along a parabolic curve  $y^2 = 4Fx$  where  $(x, y)$  is the orthogonal system of coordinates in the surface plane, the  $x$  axis is oriented along the optical axis and  $F$  is the focal length. Based on that, a mirror with  $F = 2.5$  cm was fabricated. The operational principle of the component resulted rather satisfactory. For example the expected focusing was exhibited along the axis of the mirror.

## 8. Outlook

In the area of surface plasmon polariton nano-optics many features have already been clarified. The progress in both theoretical and experimental aspects has significantly increased with the advent of the near-field optical microscopy. Thus, different regimes of SPP scattering have been experimentally observed and related to the phenomena of weak and strong SPP localization. In another hand, nano-scatterers were used to create almost any kind of conceivable SPP nanocomponent such as a line, corner square and parabolic nano-mirrors. Simple but powerful mathematical models were proposed in order to deal with the observed SPP phenomena. During the course of the research, several devices composed of a set of nano-scatterers have been numerically simulated and its stability (to geometric parameters) and dispersion dependence were studied in detail. The corresponding experimental results demonstrated that the model is accurate enough and that can be used, in straightforward manner, to design SPP nano-components. Furthermore we have designed and constructed a stand-alone SNMM, including electronics and software, and demonstrated that it works. The SNMM showed capabilities for imaging of evanescent microwaves. The technique can be used, with certain limitations, as a check for testing potential micro and nano components assembled of individual scatterers, e.g., beam-splitters and interferometers. We conduct further investigations in this area.

### Acknowledgements.

I gratefully acknowledged all my co-workers and colleagues for their invaluable contributions and discussions during the course of this research. I should also thank the support by CONACyT project SEP-2004-C01-45999.

## References

- [1] H. Raether, *Surface Plasmons*, Springer Tracts in Modern Physics Vol. 111 (Springer, Berlin, 1988). *Surface Polaritons*, edited by V. M. Agranovich and D. L. Mills (North-Holland, Amsterdam, 1982).
- [2] S. I. Bozhevolnyi and F. A. Pudonin, *Phys. Rev. Lett.* **78**, 2823 (1997).
- [3] *Near Field Optics*, edited by D. W. Pohl and D. Courjon (Kluwer, The Netherlands, 1993).
- [4] S.I. Bozhevolnyi, *Phys. Rev. B* **54**, 8177 (1996).
- [5] S.I. Bozhevolnyi and V. Coello, *Phys. Rev. B*, **58**, 10899 (1998).
- [6] S.I. Bozhevolnyi and V. Volkov, *Opt. Comm.* **198**, 241 (2001).
- [7] T.Søndergaard and S.I. Bozhevolnyi, *Phys. Rev. B*, **67**, 165405 (2003).
- [8] V. Coello, T. Søndergaard, S.I. Bozhevolnyi *Opt. Comm.* **240**, 345 (2004).
- [9] E. Ash and G. Nicholls, *Nature* **237**, 510 (1972).
- [10] T. Wei, X.-D. Xiang, W.G. Wallace-Freedman and P. G. Schultz, *Appl. Phys. Lett.* **68** 24 (1996); C.P. Vlahacos, R. C. Black, S.M. Anlage, A. Amar, and F.C. Wellstood, *Appl. Phys. Lett.* **69** 21 (1996); D.E. Steinhauer, C.P. Vlahacos, S. K. Dutta, B. J. Feenstra, F. C. Wellstood, and Steven M. Anlage, *Appl. Phys. Lett.* **72** 7 (1997).
- [11] C. Martinez, V.Coello, R.Cortes, R. Villagomez J. Korean Phys. Soc. **47** S152 (2005); V.Coello, R.Cortes, R. Villagomez, R. Lopez, C. Martinez, *Rev. Mex. de Fis.* **51** 426 (2005).
- [12] W.Barnes, W.A. Murray, J. Dintinger, E. Devaux, T.W. Ebbesen. *Phys. Rev. Lett.* **92**, 107401 (2004).
- [13] E. H. Synge, *Phil. Mag.* **6**, 356 (1928).
- [14] Lord Rayleigh, *Phil. Mag.* **42**, 167 (1896). E. Abbe, *Archiv f. mikroskop. Anat.* **9**, 413 (1873).
- [15] R. C. Reddick, R. J. Warmack, and T. L. Ferrel, *Phys. Rev. B* **39**, 767 (1989); D. Courjon, K. Sarayedine, and M. Spajer, *Opt. Commun.* **71**, 23 (1989); F. de Fornel *et al.*, *Proc. SPIE* **1139**, 77 (1989).
- [16] D. Van Labeke and D. Barchiesi, *J. Opt. Soc. Am. A* **10**, 2193 (1993); R. Carminati and J.-J. Greffet, *Opt. Commun.* **116**, 316 (1995);
- [17] V. Coello, S. I. Bozhevolnyi, and F. A. Pudonin, *Proc. SPIE* **3098**, 536 (1997).
- [18] S.I. Bozhevolnyi, A.V. Zayats, and B. Vohnsen, in *Optics at the Nanometer Scale*, eds, M.Nieto-Vesperinas and N. García (Kluwer, Dordrecht, 1996), p.163.
- [19] M.P. Van Albada,, M.B. Van der Mark, A. Lagendijk. (1990). Experiments of weak localization of light and

- their interpretation, in P. Sheng (ed.), *Scattering and localization of classical waves in random media*, World Scientific, Singapore.
- [20] A. V. Shechegrov, I. V. Novikov, and A. A. Maradudin, *Phys. Rev. Lett.* **78**, 4269 (1997).
- [21] S. I. Bozhevolnyi and F. A. Pudonin, *Phys. Rev. Lett.* **78**, 2823 (1997).
- [22] Milton Abramowitz and Irene A. Stegun. *Handbook of Mathematical Functions*, 9<sup>th</sup> printing. National Bureau of Standards (1970).
- [23] S.I. Bozhevolnyi, V.S. Volkov, and K. Leosson. *Phys. Rev. Lett.* **89**, 186801 (2002).
- [24] H. Dittlbacher, J.R. Krenn, G. Shider, A. Leitner, F.R. Aussenegg, *Appl. Phys. Lett.* **81** 1762 (2002).
- [25] V. Coello, T. Søndergaard, S. I. Bozhevolnyi , *Opt Comm* **240**, 345 (2004).